

SLUG – STOCHASTICALLY LIGHTING UP GALAXIES I: METHODS AND VALIDATING TESTS

ROBERT L. DA SILVA^{1,2}, MICHELE FUMAGALLI¹, AND MARK KRUMHOLZ¹*Draft version June 17, 2011*

ABSTRACT

The effects of stochasticity on the luminosities of stellar populations are an often neglected but crucial element for understanding populations in the low mass or low star formation rate regime. To address this issue, we present SLUG, a new code to “Stochastically Light Up Galaxies”. SLUG synthesizes stellar populations using a Monte Carlo technique that treats stochastic sampling properly including the effects of clustering, the stellar initial mass function, star formation history, stellar evolution, and cluster disruption. This code produces many useful outputs, including i) catalogs of star clusters and their properties, such as their stellar initial mass distributions and their photometric properties in a variety of filters, ii) two dimensional histograms of color-magnitude diagrams of every star in the simulation, iii) and the photometric properties of field stars and the integrated photometry of the entire simulated galaxy. After presenting the SLUG algorithm in detail, we validate the code through comparisons with SB99 in the well-sampled regime, and with observed photometry of Milky Way clusters. Finally, we demonstrate the SLUG’s capabilities by presenting outputs in the stochastic regime. SLUG is publicly distributed through the website <http://sites.google.com/site/runslug/>.

Subject headings: methods: statistical; galaxies: star clusters; galaxies: stellar content; stars: formation; methods: numerical; techniques: photometric

1. INTRODUCTION

Fundamental progress in understanding the properties of galaxies, star clusters and stellar populations comes from the comparisons between observed photometry and synthetic photometry derived from stellar evolution codes. It has become common practice to infer properties such as star formation rate (SFR), star formation history (SFH), age, metallicity, redshift, and stellar mass from photometry. Despite the limits of theoretical modeling of stellar populations (such as uncertainties with dust, stellar evolution, and the stellar initial mass function (IMF); see Conroy et al. 2009, 2010; Conroy & Gunn 2010) synthetic libraries have reached a degree of precision that allows accurate estimates of these parameters – although sometimes with degeneracy – in massive galaxies and clusters.

However, observations reveal a higher complexity in lower mass systems where scaling relations which apply to more massive systems cannot be trivially extrapolated (e.g., Lee et al. 2007; Weisz et al. 2008). Moreover, in lower mass systems, the limited number of stars that are present invalidates the basic assumption used by most of the currently available codes for synthetic photometry (such as STARBURST99 (SB99; Leitherer et al. 1999); PEGASE (Fioc & Rocca-Volmerange 1997); and GALEV (Kotulla et al. 2009)): that the IMF is fully sampled at all times. Violation of this assumption leads to stochastic variations in photometric properties that these codes do not fully capture.

For example in globular clusters, the simplest observed stellar populations, failure to account for sampling effects can lead to a dramatic overestimate of the contributions of blue horizontal branch and AGB stars to the

integrated light. As a result, correct estimates of globular cluster ages and metallicities based on their integrated light are possible only if one correctly accounts for stochasticity (Colucci et al. 2011).

Moreover, in weakly star forming regions, stochastic effects can mimic those of a varying IMF. Indeed, recent observations in the low SFR regime have led to serious consideration of a varying IMF (Pflamm-Altenburg & Kroupa 2008; Hoversten & Glazebrook 2008; Meurer et al. 2009; Lee et al. 2009). However a fully self-consistent model of stochasticity, allowing for a full range of parameters such as differing degrees of stellar clustering, metallicities, stellar tracks, input IMFs and CMFs, and SFHs has not been available to test the null hypothesis of a non-varying but stochastically sampled IMF.

These considerations apply not only to the dwarf galaxies studied by Lee et al. (2009) but also to the outer regions of galaxies such as XUV disks (Boissier et al. 2007a; Thilker et al. 2007) and outlying H II regions (Werk et al. 2008; Gogarten et al. 2009) where stochasticity becomes crucial in the interpretation of inferred SFRs and SFHs.

While the number of studies that use Monte Carlo approaches to address problems on scales of clusters and galaxies is growing, a general purpose tool to study photometry in clusters and galaxies has not previously been available. To fill this need, we have created SLUG, a code to allow proper study of the stochastic star formation regime at a range of scales from individual star clusters to entire galaxies. SLUG provides a variety of tools for studying the stochastic regime, such as the ability to create catalogs of clusters including their individual IMFs and photometric properties, color-magnitude diagrams (CMDs) of entire galaxies where we keep track of the photometry of every star, as well as integrated photometry of entire composite populations.

¹ Department of Astronomy and Astrophysics, UCO/Lick Observatory, University of California, 1156 High Street, Santa Cruz, CA 95064

² NSF Graduate Research Fellow

This paper, the first of a series, focuses on the methods used in the code along with several tests to demonstrate that we are reliably reproducing observations and other synthetic photometry predictions. We then demonstrate the use of this code in the stochastic regime. In a companion paper (Fumagalli et al. 2011), we use SLUG to demonstrate that, once random sampling is included, a stochastic non-varying IMF can reproduce the observed variation of the $H\alpha$ /FUV ratio in dwarf galaxies without resorting to modifications of the IMF. In the second paper of the series (da Silva et al in prep.) we will explore in detail the implications of stochastic star formation with clustering. Further work will apply this code to a variety of astrophysical questions, such as understanding SFR calibrations in the stochastic regime and further study of other claims of a varying IMF.

The layout of the paper is as follows: §2 presents an introduction to stochasticity and its effects on the luminosity of stellar populations; §3 gives a detailed description of the SLUG algorithm; §4 discusses various tests of the code; §5 shows a presentation of the code’s outputs in the stochastic regime; finally, §6 summarizes the results.

2. WHAT IS STOCHASTICITY?

Many astrophysical studies require creation of synthetic photometry of galaxies and other collections of stars in order to compare with observations. In this section we present a discussion of the various effects of stochasticity and the regimes in which they are important.

2.1. Coeval Stellar Populations

The standard procedure for calculating the luminosity from a coeval population of stars used by the most popular implementations (such as SB99) is as follows. To find the luminosity per unit mass of a coeval population in some band β at a time t after formation ($\ell_{\beta, \text{coeval}}(t)$), one simply integrates the luminosity per unit mass of each star in that band as a function of mass and time ($\ell_{\beta}(m, t)$) weighted by the distribution of stellar masses (i. e. the IMF) $\frac{dN}{d \ln m}$:

$$\ell_{\beta, \text{coeval}}(t) = \int_{m_{\min}}^{m_{\max}} \ell_{\beta}(m, t) \frac{dN}{d \ln m} dm. \quad (1)$$

Note that here we use a normalization of the IMF such that $\int_{m_{\min}}^{m_{\max}} \frac{dN}{d \ln m} dm = 1$.

By performing this integral, these models assume an infinitely well-sampled IMF. As a result the above formula is mass-independent, meaning that $\ell_{\beta, \text{coeval}}$ can be scaled according to the total amount of stellar mass in a population (i.e. the luminosity of a mass M of stars is simply $M \ell_{\beta, \text{coeval}}$). Thus a given amount of mass M will have a 1-to-1 mapping to a particular luminosity L . However for small stellar populations, the assumption of continuous sampling breaks down and effects of stochasticity can become important. Specifically, stochastic effects create a statistical dispersion of luminosities that result from a given mass M of stars based entirely on the probabilistic sampling of the mass distribution of stars. This is because each realization of a given mass M is built up with a different distribution of stellar masses which, due to the non-linear dependence of luminosity on stellar

mass, yields a different luminosity. We call this type of stochastic process *sampling stochasticity*.

Perhaps the most important manifestation of sampling stochasticity is undersampling of the upper end of the IMF. Since the IMF is steeply declining with increasing stellar mass, the expectation value of a low mass population drawing a massive star is small. As a result, the IMF in a low mass population with few stars can appear truncated and have less luminosity than a fully-sampled assumption would have predicted. This is due to the very super linear dependence of luminosity on stellar mass.

One can roughly estimate the mass below which this effect is insignificant by calculating the expectation value of obtaining a star above a given mass. We do so following the formalism of Elmegreen (2000), who find that the total mass (M) required to expect a single star above a mass m is

$$M \sim 3 \times 10^3 \left(\frac{m}{100 M_{\odot}} \right)^{1.35}. \quad (2)$$

This statement is clearly dependent on one’s choice of IMF. Elmegreen (2000) uses a Salpeter IMF with a lower limit of $0.3 M_{\odot}$ and no upper limit. If one imposes an upper limit to the stellar mass function, this relation turns over and asymptotically approaches the limit. However, for order-of-magnitude purposes here, we neglect such consideration. This result implies that in order to reasonably expect even a single $120 M_{\odot}$ star³, one would need at least a total mass sampled of approximately $10^4 M_{\odot} \equiv M_{\text{trunc}}$. Thus this IMF truncation effect of sampling stochasticity can be ignored for *coeval* populations with masses $\gg M_{\text{trunc}}$. For more reference on the limits of stochastic sampling, we recommend Cerviño & Valls-Gabaud (2003) and Cerviño et al. (2003). For specific considerations to $H\alpha$ luminosity (one of the features of a stellar population most sensitive to stochasticity), see Cerviño & Luridiana (2004).

Another manner in which stochastic sampling can manifest in coeval populations is for stars going through particularly short-lived and luminous phases of evolution after they leave the main sequence (e.g., AGB and blue horizontal branch stars). Since these phases are short, only a very narrow range of masses is undergoing one of them at any given time. Thus the exact sampling within that mass range can have a large impact on the number of stars within that phase. As a result, a non-infinite population of stars can have additional random scatter in luminosity even if $M > M_{\text{trunc}}$. This effect is more important in populations with little ongoing star formation relative to their stellar mass (otherwise new stars dominate the photometric properties of the population), at specific ages when these post-main sequence populations contribute significantly to the luminosity of the population (Colucci et al. 2011).

2.2. Composite Stellar Populations

In order to characterize a more complicated star formation history, SB99 and other such schemes integrate

³ Due to limitations of stellar evolutionary tracks, this is the highest stellar mass SLUG can model and is a reasonable guess for the highly uncertain absolute stellar mass limit. While some (e.g., Figer 2005) suggest a value of $\sim 120 - 150 M_{\odot}$ others (Crowther et al. 2010) suggest it may be as high as $300 M_{\odot}$.

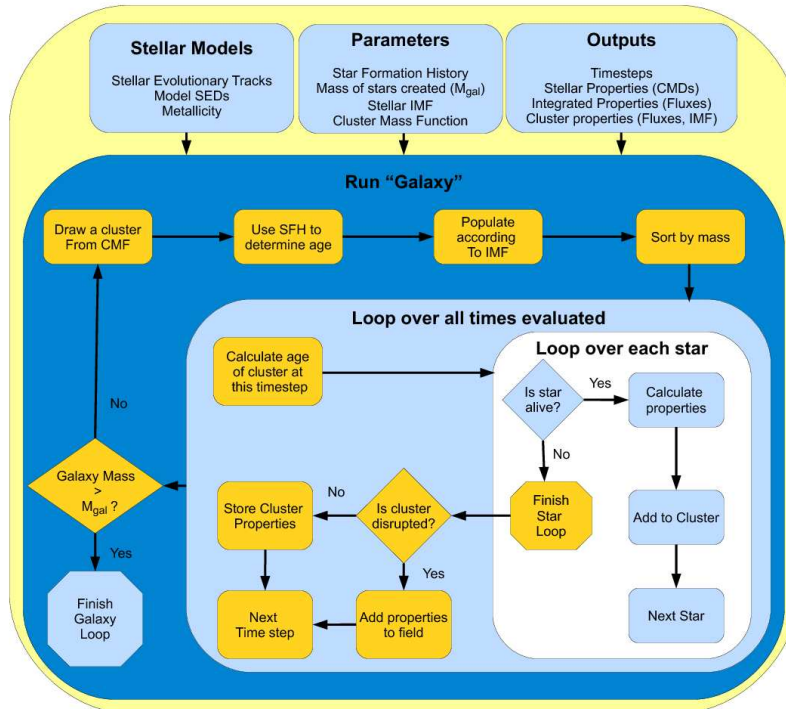


FIG. 1.— A schematic flow-chart describing the algorithm of the the SLUG code. Note that for the case of unclustered star formation, the cluster mass is drawn from the IMF and the population step is skipped as the single star is treated as part of a disrupted cluster for the remainder of the code. Note this is updated from Fumagalli et al. (2010).

over the coeval populations discussed above to find the luminosity of all stars in a given band at a time τ ,

$$L_{\beta, total}(\tau) = \int_{-\infty}^{\tau} \text{SFR}(t) \ell_{\beta, coeval}(\tau - t) dt. \quad (3)$$

Such a treatment makes two key assumptions: (1) each of the summed coeval populations is large enough to ignore the effects of sampling stochasticity and (2) the SFR is continuously sampled as well. These assumptions can quickly break down for sufficiently low SFRs.

To illustrate this point, consider a galaxy forming stars at a constant rate. In order for the IMF not to be truncated within some time interval dt , there need to be at least M_{trunc} worth of stars formed in that interval. For the SFR to be considered reasonably well sampled, dt must be much smaller than the evolutionary timescales of any of the stars, which are $\approx 10^6$ yr for the massive stars that generally dominate the light in an actively star-forming system. Thus these assumptions require

$$dt = \frac{M_{trunc}}{\text{SFR}} \ll 10^6 \text{ yr}. \quad (4)$$

Thus these effects can only be ignored for SFRs consistently $\gg 10^{-2} M_{\odot} \text{ yr}^{-1} \equiv \text{SFR}_{temp}$. However, this *temporal* stochasticity is amplified when one considers that stars are believed to be formed in discrete collections known as clusters. As a result, the clumping in time of star formation in clusters can produce stochastic effects even in regions with SFRs higher than SFR_{temp} . In this case the characteristic mass in Equation 4 is replaced with a mass characteristic of the clusters being drawn (discussed further in da Silva in prep.; Fumagalli et al. 2011).

The conditions required to treat a stellar population as continuous (as opposed to stochastically sampled) break down in a variety of astrophysical environments such as dwarf galaxies (e.g., Lee et al. 2009), low star formation rate regions in the outskirts of galaxies (e.g., Boissier et al. 2007b; Fumagalli & Gavazzi 2008; Bigiel et al. 2010), and low surface brightness galaxies (e.g., Boissier et al. 2008).

3. TECHNIQUE

3.1. Overview

Here we present a brief overview of the code while we present each step in detail in the subsequent sections.

SLUG simulates star formation according to the scheme presented in Figure 1. We create collections of star clusters obeying a user-defined cluster mass function (CMF) (which can include a given mass fraction of stars not formed in clusters), SFH, IMF, and choice of stellar evolutionary tracks, which we call a “galaxy”. A description of the parameters that users can vary is provided in Table 1.

These galaxies are built up (§3.2) by first drawing the mass of an individual cluster from a CMF. This cluster’s mass is then filled up with stars according to an IMF. The age of the cluster is drawn from a distribution weighted by the given SFH. Each of the stars within the cluster is evolved using a stellar evolutionary track combined with a model spectral energy distribution (SED) to determine a variety of integrated fluxes corresponding to commonly used photometric filters (§3.3).

At a given set of time steps, these fluxes are summed over each star cluster. The clusters are then disrupted according to the prescription of Fall et al. (2009a). Dis-

TABLE 1
INPUT PARAMETERS

Parameter	Description
Controlling the Physics	
IMF	stellar initial mass function; can choose Kroupa, Salpeter, Chabrier, IGIMF, or an arbitrary slope
CMF	cluster mass function, can change slope, minimum and maximum mass
Stellar Evolutionary Tracks	library of models used for stellar evolution
Metallicity	metallicity of the stellar population
Stellar Atmosphere	which scheme and models are used for SEDs
Stellar Wind Model	which wind model is used for SEDs
Fraction of stars in clusters	mass fraction of stars formed in clusters
Controlling the Simulation	
Maximum time	how long the simulation is run
SFH	can be arbitrary
Seed	random seed used for simulation
Controlling Output	
Time step	time between code outputs
Fluxes	choose which fluxes to output
Colors	which colors to use for CMDs
CMD output parameters	choice of number of bins and range of color and luminosity for each CMD
Cluster output?	set to print output for each cluster
IMF output?	set to output IMF histograms for each cluster

rupted clusters have their fluxes added to a “field” population while surviving clusters have their properties stored individually. The code repeats this process until a stellar mass equal to the integral of the provided SFH is created.

The code outputs a variety of files that keep track of the properties of the stars, clusters, and total integrated stellar populations. Table 2 provides a short description of each available output file. All outputs are parsed and transformed into binary FITS tables.

The code is open source and written in C++ with wrapping and parsing routines written in IDL. This entire process can be controlled through an IDL graphical user interface (see Figure 2) or either of the UNIX or IDL command lines. The IDL routines are wrapped in packages for use with the IDL virtual machine⁴ for those without IDL licenses. For a full manual on how to use the code, visit the SLUG website at <http://sites.google.com/site/runslug/>.

3.2. Cluster Creation

Most stars are thought to be born in star clusters (Lada & Lada 2003) and the distribution of star cluster masses appears to obey a power law distribution, where observations (e.g., Zhang & Fall 1999; Lada & Lada 2003; Fall et al. 2009b; Chandar et al. 2010) and theory

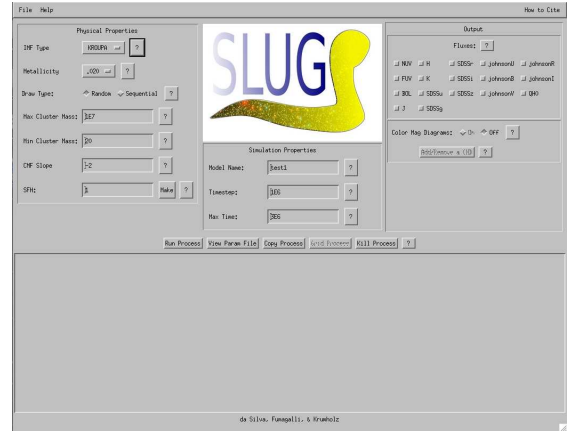


FIG. 2.— IDL GUI interface for running the code. The code may also be called via the UNIX or IDL command lines.

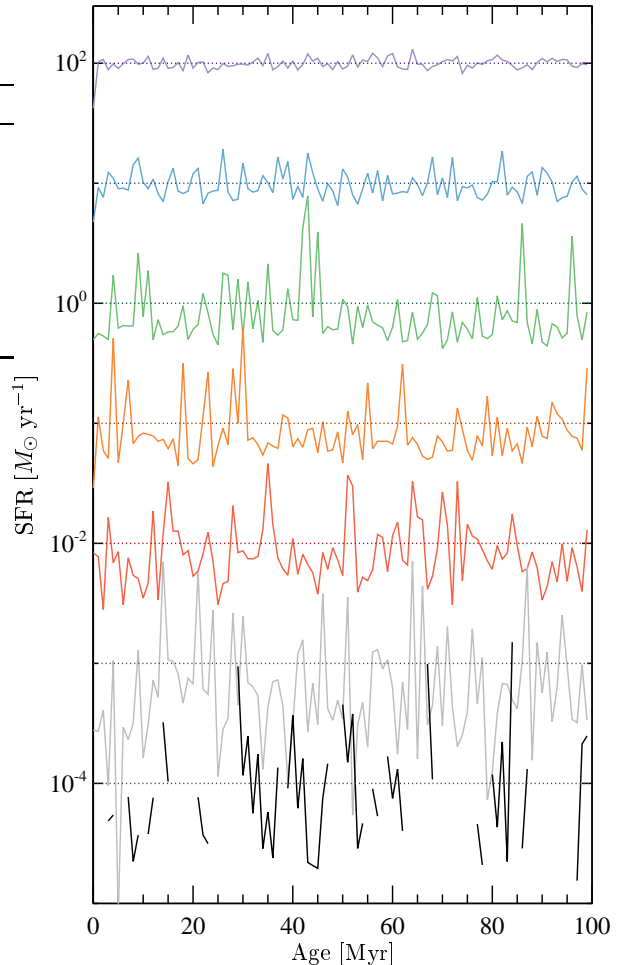


FIG. 3.— Examples of star formation histories average over 1 Myr bins for simulations with varying input constant SFRs of 0.0001–100 $M_{\odot} \text{ yr}^{-1}$. The dotted lines show the input SFR. The average SFR of the simulation in each case is within 2, 0.2, and <0.02 percent of the input for 10^{-4} , 10^{-3} , and $>10^{-2} M_{\odot} \text{ yr}^{-1}$ respectively. SFRs of zero are masked.

⁴ which is available for free from <http://www.itvis.com/language/en-us/productsservices/idl/idlmodules/idlvirtualmachine.aspx>

TABLE 2
SLUG OUTPUT FILES

Name	Description
Histogram	a 2d histogram of the user’s choice of color-magnitude diagram(s) of every star in the “galaxy” at each timestep
Cluster	mass, fluxes, most massive star, number of stars, and age of each undisrupted cluster at each timestep
IMF	a histogram of the IMF of each cluster that appears in the Cluster file
Integral	the total flux of the entire “galaxy” at each timestep
Miscellaneous	the total stellar mass actually formed, as well as the actual SFH and CMF of the simulation

(e.g., Fall et al. 2010) suggest that the index (β) of the power law $dN/dM \propto M^{-\beta}$ is approximately 2. SLUG allows for both clustered and unclustered star formation. The user can choose what fraction of all stellar mass they wish to form in star clusters. If the code is forming clusters, the CMF’s power law slope as well as its upper and lower bounds can be varied. If unclustered star formation is desired, the stars’ masses are drawn individually from an IMF and treated as a disrupted “cluster” of one star for the remainder of the code.

The initial masses of stars are drawn from an IMF. Choices of IMF⁵ currently are Chabrier (2003), Kroupa (2001), Salpeter (1955), a user-defined arbitrary power law, and the recently proposed IGIMF (Kroupa & Weidner 2003; Pflamm-Altenburg & Kroupa 2008). While the Chabrier, Kroupa, Salpeter, and power law IMFs are implemented as a standard probability density function of stellar masses, the IGIMF has additional features that require different treatment (see Appendix A).

Regardless of the choice of IMF, we draw stars until the total mass of the star cluster is built up. Since the random distribution of stars never exactly equals the mass of the cluster, a question arises as to whether to keep the last star added. This last star increases the mass of the cluster above the cluster mass drawn from the CMF. We determine whether or not to keep that star in the cluster based on whether keeping the star in makes the total mass of stars closer to the mass drawn from the CMF than leaving it out⁶.

Independent of its mass, the age of the cluster relative to the galaxy is assigned in a probabilistic manner weighted by the SFH (which can be arbitrary) such that the SFH is reproduced on average. This produces a scatter in the SFHs for even a given “constant” SFR. Thus SLUG’s definition of a galaxy with a constant SFR is not a galaxy where the SFR is constant at every individual time⁷, but rather a galaxy that produces an amount of stars over a time dt equal to $\text{SFR} \times dt$ which are distributed in clusters whose ages are drawn from a uniform distribution. This interpretation of what a SFR is and its implications is discussed in more detail in da Silva et

al. (in prep.).

Clusters are born until the total mass of stars formed is equal to the integral of the SFH. As with the problem of populating a cluster with stars, a galaxy will never be filled to exactly its given mass with an integer number of clusters. Therefore we apply the same condition for populating the galaxy as we do the clusters: we add until we exceed the mass and keep the final cluster only if the total galaxy mass is closer to the desired value if we keep it. As a result the average SFR over the entire simulation of a particular galaxy can be higher or lower than the input value. This effect is small for most regimes, but very rare drawings of the CMF at low SFRs can produce mild departures. We emphasize that this is not the effect of any error associated with the code but rather is the necessary result of our interpretation of what a SFR means.

We demonstrate the results of this procedure in Figure 3. The figure shows that, while lower average SFRs tend to produce larger fractional scatter in the instantaneous SFR, significant scatter remains until SFRs exceed $10 M_{\odot} \text{ yr}^{-1}$. This scatter is a direct result of the finite size of clusters. To clarify with an example, consider that a $10^7 M_{\odot}$ cluster (when averaged over the 1 Myr similarly to the curves shown in Figure 3), will appear as a deviant peak for all but the highest SFRs, where the contribution of that individual cluster is drowned out by enough other clusters.

We note that in this release of the code all stars in a cluster are treated as having identically the same age. While observations suggest a scatter of a several Myr (Palla & Stahler 1999; Jeffries 2007; Hosokawa et al. 2011), the mass dependence of this scatter is unclear. Given the uncertainties, and that the intracluster age scatter is at most a few Myr, we chose to neglect this effect for now but plan on implementing it in the future.

3.3. Stellar Tracks, SEDs, and Broad Band Photometry

Given the mass and age of each star, we need to determine its properties for a variety of observables. Our method uses many of the same algorithms found in SB99 (Leitherer et al. 1999; Vázquez & Leitherer 2005) to create a set of tables from which SLUG interpolates. These tables are constructed in advance so they need not be computed at run time.

Our first step is to determine the physical properties of each star. To this end, we make use of a variety of stellar evolutionary models. Modifying the SB99 source code, we were able to obtain the full range of stellar tracks available to SB99 (see Table 3). In the future we plan to implement a wider range of stellar tracks including

⁵ IMFs are truncated at $0.08 M_{\odot}$ due to lack of lower mass stellar tracks

⁶ The effects of different sampling methods and their dependence on the CMF is studied in detail by Haas & Anders (2010). Our method is identical to their ‘stop-nearest’ method.

⁷ A constant SFR cannot be instantaneously constant because stars form in discrete units of mass. For example, when a star is born, the instantaneous SFR is infinite, thus we must turn to a more probabilistic interpretation of the SFR.

those from Eldridge & Stanway (2009) and the BaSTI library (Pietrinferni et al. 2007; Cordier et al. 2007). We supplement the Geneva tracks with the Padova+AGB tracks for stars in the mass range $0.15\text{--}0.8 M_{\odot}$. These models provide luminosities, gravities, chemical compositions, and effective temperatures at discrete intervals in the evolution of a discrete number of stellar masses. We then need to map these physical properties to stellar atmospheres in order to estimate the spectral energy distributions of the stars. Our code allows users to choose from one of five possible SB99 algorithms for modeling the atmospheres. We implement all four prescriptions of stellar winds available in SB99 (Maeder, empirical, theoretical, and Elson), which affect the SEDs for Wolf-Rayet stars for some regimes and prescriptions. It is important to note that the SB99 algorithms match SEDs to tracks with a nearest neighbor approach and not through interpolation. Therefore there can be some discreteness in the output SEDs. Future work will include removal of this effect.

With SEDs in hand, we can convolve with filters to determine the photometry of each point in our stellar tracks. For this step we include the effects of nebular continuum (free-free, free-bound, and 2 photon processes) as implemented in SB99, but neglect nebular line emission for this first release of the code. (For a discussion of the importance of nebular continuum for the SEDs, see Reines et al. 2010. Also see Leitherer & Heckman 1995 and Mollá et al. 2009.) The full list of available filters is presented in Table 4. We also integrate the SED to determine the bolometric luminosity as well as to calculate $Q(H^0)$, the number of hydrogen ionizing photons emitted per second. One can convert $Q(H^0)$ to $H\alpha$ luminosity with a simple conversion assuming case B recombination (our notation follows Osterbrock & Ferland 2006).

$$L_{H\alpha} = (1 - f_{esc})(1 - f_{dust})Q(H^0) \left(\frac{\alpha_{H\alpha}^{eff}}{\alpha_B} \right) h\nu_{H\alpha} \\ \approx 1.37 \times 10^{-12} (1 - f_{esc})(1 - f_{dust})Q(H^0) \text{ ergs/s} \quad (5)$$

where f_{esc} is the escape fraction (thought to be between 0.05 (Boselli et al. 2009) and 0.4 (Hirashita et al. 2003)) and f_{dust} represents the fraction of ionizing photons absorbed by dust grains (e.g., see appendix of McKee & Williams 1997, who suggest a value of 0.37). To better characterize the ionizing luminosity we also keep track of $Q(He^0)$ and $Q(He^1)$ which represent the numbers of ionizing photons in the He I and He II continua respectively.

The above steps allow us to create a discrete two-dimensional table for each flux band where one axis represents stellar mass, the other represents time, and the value of the table is the logarithm of the flux in that band at the appropriate mass and time. Our tables are created through use of the isochrone synthesis method such that our results are stable against the numerical issues that arise from a fixed mass approach (Charlot & Bruzual 1991).

3.4. Evaluating the Stellar Properties

To determine the properties of a given star of any mass at any given time, we first determine if the star is still

alive. This is done by an interpolation in time to find the minimum mass of a dead star (m_{death}) at a given time according to our stellar evolution models (where we call a star “dead” if it no longer has entries in our stellar tracks). If the star is less massive than m_{death} , we interpolate our model tables to determine the flux in a given filter within 0.01 dex.

For computational speed, there are a variety of approximations and restrictions we are forced to implement. The current scheme only allows ages up to 1 Gyr for the stellar tracks (to be expanded in later releases of the code). We do not evolve stars less massive than $0.9 M_{\odot}$ (a number which can be changed by the user). These stars do not evolve past the main sequence for the current maximum age of the code of 1 Gyr, so these stars are treated as having their zero-age main sequence (ZAMS) properties. Due to limitations of the stellar tracks, we treat the photometric properties of all stars less massive than $0.156 M_{\odot}$ identically to those of $0.156 M_{\odot}$ stars. For many purposes, more massive stars dominate the light in the bands such that this approximation is reasonable. The tracks also impose a $120 M_{\odot}$ upper mass limit on stars.

Currently, we neglect the effects of binary stellar evolution (see Eldridge & Stanway 2009), which may have an impact on the derived results by producing a bluer population with a reduced number of red supergiants and increased age range of Wolf-Rayet stars.

3.5. Cluster Disruption

If the user chooses to form stars in star clusters, we randomly disrupt our clusters in a mass independent way such that $dN/d\tau \propto \tau^{-1}$ (following Fall et al. 2009a). We start cluster disruption 1 Myr after the cluster forms. This results in 90% of star clusters being disrupted for each factor of 10 in age after 1 Myr. Stars in disrupted clusters still have their photometry calculated for the integrated properties of the galaxy and are kept track in a set of “field” variables and outputs.

4. VALIDATING TESTS

In this section we present a variety of tests to validate the outputs of SLUG. For these tests we make use of a set of fiducial parameters presented in Table 5 unless otherwise noted^{8,9}. To emphasize that SLUG can be applied at different scales, we arrange these tests in order of scale starting with individual clusters and then considering integrated properties of entire galaxies in the well-sampled regime.

4.1. Photometry of Clusters

To demonstrate that SLUG reproduces properties of observed clusters, we turn to the catalog of young star clusters compiled in Larsen (1999). To reproduce the clusters we modify our fiducial IMF to extend down to $0.08 M_{\odot}$ and run a SLUG model with a SFR of $1 M_{\odot}$

⁸ While the preferred SEDs for SB99 are the Pau+Smi atmospheres, we find that the Pauldrach models are far too discrete. Therefore while we provide the Pau+Smi atmospheres, we recommend the Lej+Smi.

⁹ Since we aim to test SLUG rather than to perform a study of the effects that the multiple parameters have on the luminosity distributions, we choose widely adopted values.

TABLE 3
STELLAR PROPERTIES

Parameter	Allowed Values
Tracks	Geneva STD ^a , Geneva High ^a , Padova STD ^b , Padova AGB ^b
Metallicity^c	0.0004-0.50
SEDs	Planck ^d , Lejeune ^e , Lejeune+Sch ^f , Lejeune+SMI ^g , Pau+SMI ^h
Wind Models	Maeder ⁱ , Empirical ⁱ , Theoretical ⁱ , Elson ⁱ

^a Meynet et al. (1994) and references therein

^b Fagotto et al. (1994) and references therein

^c solar is 0.20

^d simple blackbody SED

^e Lejeune et al. (1997, 1998)

^f same as e, but for stars with strong winds use Schmutz (1998)

^g same as e, but for stars with strong winds use Hillier & Miller (1998)

^h same as g, but use Pauldrach et al. (2001) for O stars

ⁱ Leitherer et al. (1992)

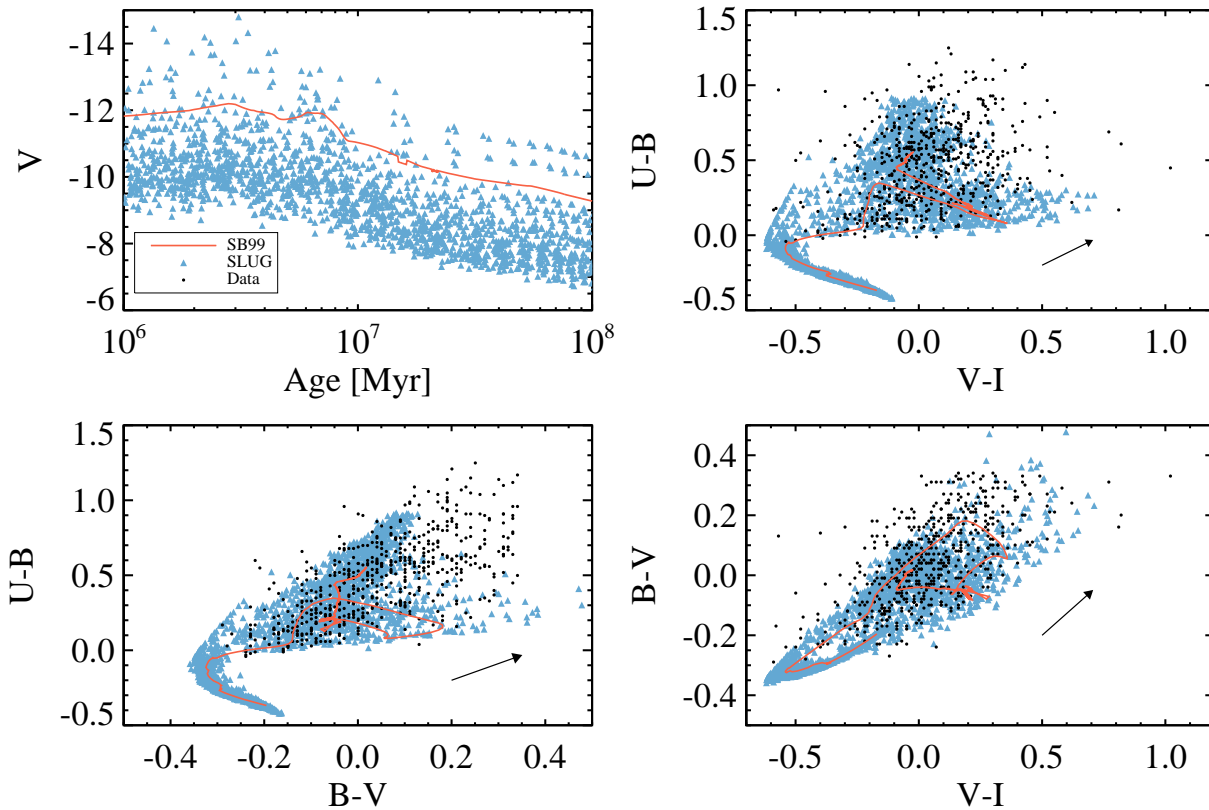


FIG. 4.— Comparison of observed young star clusters from Larsen (1999) (black points) to SLUG models of clusters $> 10^4 M_\odot$ (blue triangles). The orange curve shows the trajectory of a SB99 $10^5 M_\odot$ cluster. Data are omitted from upper left panel as the ages are not present in the Larsen (1999) catalog. Arrows denote the extinction vector for $A_V = 0.5$ mag (created following appendix B of Schlegel et al. 1998).

yr^{-1} for 500 Myr, evaluated every 10 Myr. Note that the the SFR does not directly affect the CMF or the properties of the clusters, only the number of clusters in existence at a given time. We show the results of this exercise in Figure 4 where we find remarkable agreement between the models and the data. As is clear from the figure, we are able to reproduce both the location and spread of most of the observed data. Clusters that fall outside of the locus of SLUG models fall can easily be reproduced when one accounts for a modest amount of reddening (see reddening vector).

4.2. Cluster Birthline

Another test of the photometry of clusters is to compare their $H\alpha$ luminosity to their bolometric luminosity. Work by Corbelli et al. (2009) has shown that newly born clusters lie along a birthline in this parameter space. In Fig. 5 we compare the same models as Section 4.1 (assuming f_{esc} and $f_{\text{dust}} = 0$) with their observational data and find good agreement. Our theoretical predictions differ slightly in the tilt of the locus of points from those by Corbelli et al. (2009), since we characterize the properties of our stars in a different manner (making use of stellar tracks rather than fitting formulae). To better

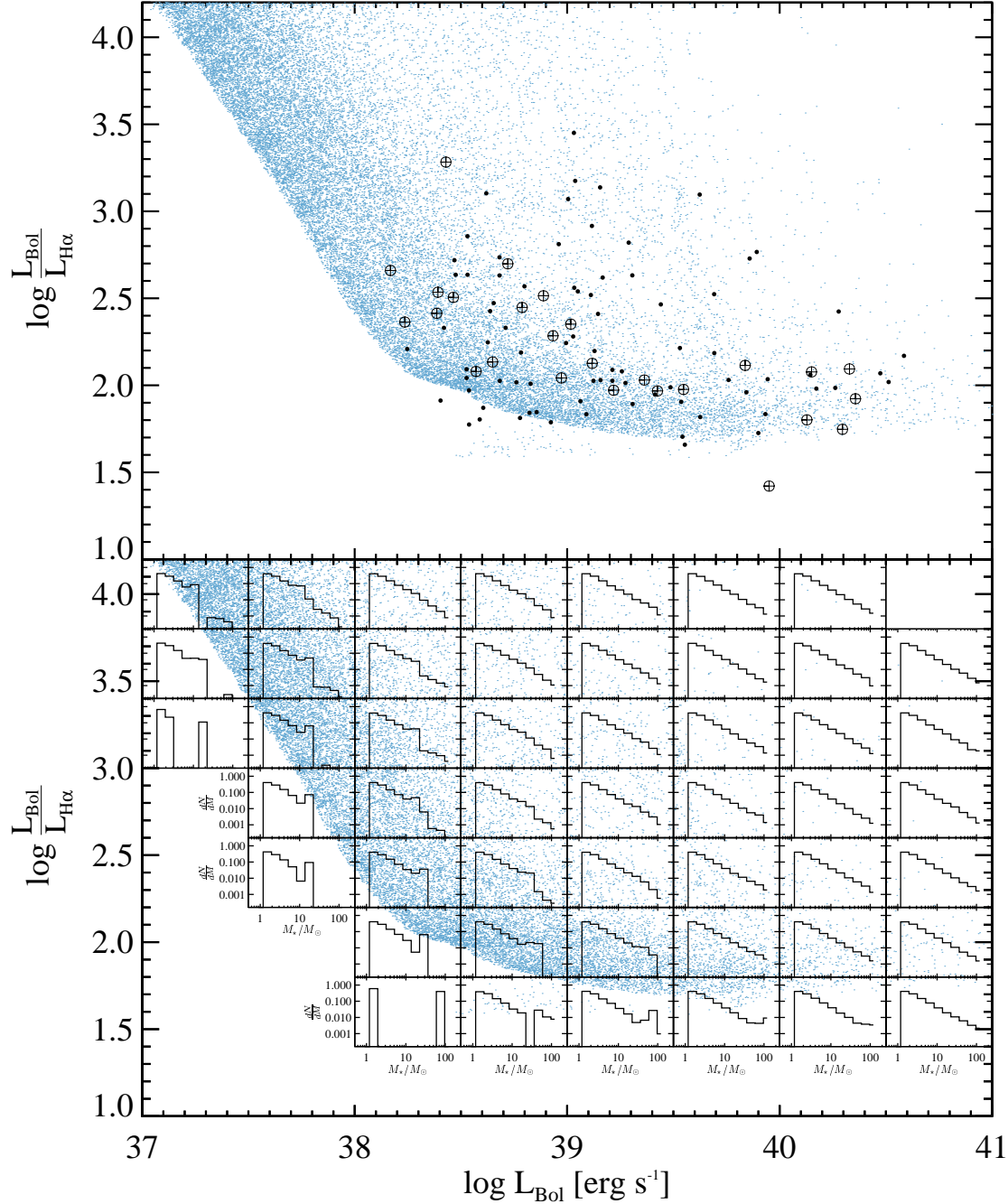


FIG. 5.— (*top*) Here we present the birthline as first discussed by Corbelli et al. (2009). Black points and crosses are data from that paper with circle-crosses denoting their ‘clean’ sample. Blue data points are clusters from SLUG. We see that our models are in relatively good agreement with observations. (*bottom*) We present overlays demonstrating the average IMFs in each region of the birthline plot.

demonstrate the origin of the birthline we also make use of SLUG’s ability to keep track of the IMF of each individual cluster (see bottom panel of Figure 5). Here we can see that the birthline from left to right forms a sequence of progressively more well-sampled upper ends of the IMF. Extremely rare deviants exist below the birthline where more extremely massive ($> 100M_{\odot}$) stars are drawn than average, resulting in being born below the birthline. Note that these rare clusters consisting of

essentially isolated O stars have also been reported in the Milky Way (de Wit et al. 2004, 2005) and the SMC (Oey et al. 2004; Lamb et al. 2010) in numbers consistent with stochastic sampling of the IMF.

4.3. Comparison with SB99

A third obvious comparison for SLUG is SB99 itself. Since SB99 is widely used, it serves as a benchmark for SLUG. Indeed, one of the motivations for making use of

TABLE 4
BROAD BAND FILTERS

Filter	Reference
NUV	1
FUV	1
<i>u</i>	2
<i>g</i>	2
<i>r</i>	2
<i>i</i>	2
<i>z</i>	2
J	3
H	3
K	3
U	4
B	4
V	4
R	4
I	4
Q(H ⁰)	5
Q(He ⁰)	5
Q(He ¹)	5
<i>L</i> _{BoI}	6

¹ Morrissey et al. (2005)

² Fukugita et al. (1996)

³ Skrutskie et al. (2006)

⁴ Appenzeller et al. (1998)

⁵ Obtained by integrating SED blueward of 912, 504, and 208 Å for Q(H⁰), Q(He⁰), Q(He¹) respectively.

⁶ Given by stellar evolutionary tracks.

TABLE 5
FIDUCIAL INPUTS

Parameter	Fiducial Value
Time step	10 ⁶ yr
Maximum time	10 ⁹ yr
IMF	1-120 <i>M</i> _⊙ ; slope=-2.35
CMF	20 - 10 ⁷ <i>M</i> _⊙ ; slope=-2
Stellar Evolutionary Tracks	Padova+AGB
Metallicity	Solar; <i>Z</i> = 0.20
Stellar Atmosphere	Lej+Smi
Stellar Wind Model	Maeder
Fraction of stars in clusters	100%

the SB99 tracks and SED matching algorithms is that our code should be able to exactly reproduce SB99 if we select input parameters that place us in the continuously-sampled regime. To that end we now present a variety of tests where we compare to SB99 to demonstrate that we can reproduce their results in this regime (the regime of a large galaxy-sized amount of stars).

To compare the outputs of both SB99 and SLUG, we choose an instantaneous burst of star formation to demonstrate the matching of the codes in both amplitude and time. We run a SB99 model similar to our fiducial model (i.e. IMF slope of -2.35 from 1-120 *M*_⊙, solar metallicity, Padova+AGB tracks, Lej+SMI SEDs, and Maeder stellar wind models). To meaningfully compare with SB99 we must choose SLUG input parameters such that we are evaluating a population where SB99's approximations are valid. We therefore draw a very large instantaneous population of 10⁹ *M*_⊙. To nullify any possible effects of our procedure for populating the clusters,

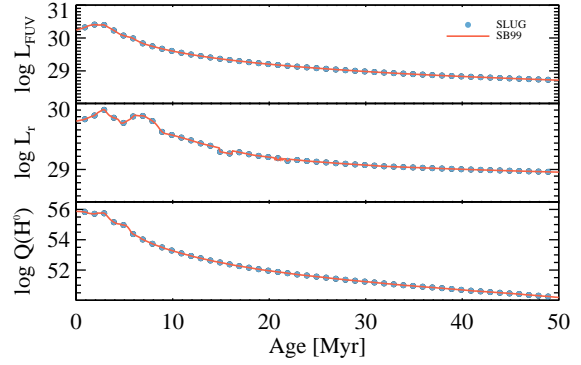


FIG. 6.— A comparison of SLUG and SB99 simulations of an instantaneous burst of 10⁹ *M*_⊙. We find good agreement between the two in both the absolute normalization of the fluxes as well as the time-dependent behavior. FUV and *r* band fluxes are presented in units of ergs/s/Hz while Q(H⁰) is in units of photons/s. In the *L_r* panel, one can see the effects of the discrete SED matching techniques implemented by SB99 in the age ranges of 12-18 Myr and 20-22 Myr.

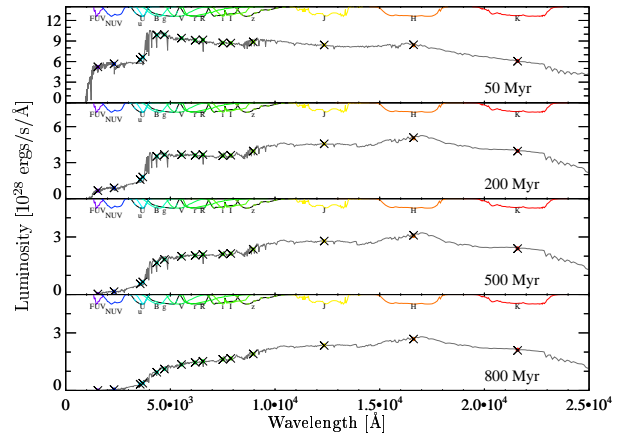


FIG. 7.— A comparison of SLUG and SB99 photometry for an instantaneous burst of 10⁹ *M*_⊙, evaluated at the ages indicated in each panel. The grey solid line represents the output spectrum from SB99 for such a population. The filled color circles show the SB99 integrated fluxes for the filters available to SLUG. The black 'x's mark the SLUG photometry for the well-sampled model described in section 4.3.

we ensure all clusters are very large by modifying the fiducial CMF to a restricted range (10⁶ - 2 × 10⁶ *M*_⊙). We present the results in Fig. 6. It is evident that we are accurately able to reproduce SB99 in the well-sampled regime for integrated “galaxy” properties. We match both the amplitude and time evolution in all photometric bands.

This can also be seen by looking at the full SEDs. In Figure 7, we present photometry for all 15 of the flux bands available for SLUG and compare with the spectra and integrated photometry produced by SB99 at a variety of time steps. Again we are able to fully reproduce the photometric properties in the well-sampled regime from FUV to *K*-band.

In both these demonstrations, SLUG matches SB99 within 0.026 dex for all fluxes at all times.

5. STOCHASTICITY IN ACTION

Having demonstrated that SLUG can reproduce realistic clusters as well as reproduce SB99's results, we now present outputs of SLUG in the stochastic regime.

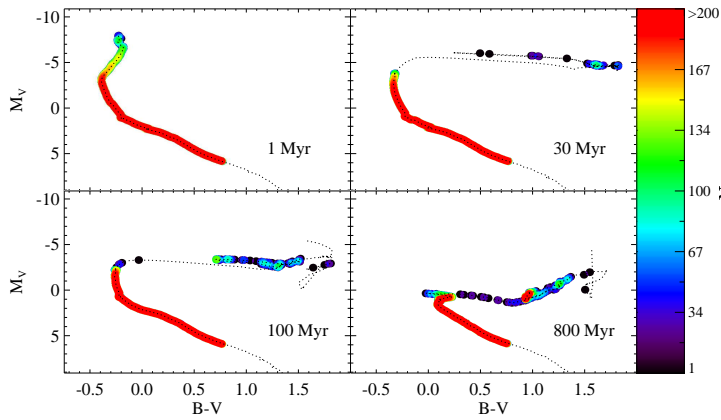


FIG. 8.— CMDs of an instantaneous $10^5 M_\odot$ burst population at the ages indicated in each panel. Only stars more massive than $0.9 M_\odot$ are binned in the CMDs. The dotted lines show the corresponding theoretical isochrones. The SLUG CMD has been convolved with circular top-hat PSF solely to improve visibility. The color bar denotes the number of stars in that region of the diagram.

5.1. Effects on Coeval Populations

Recent studies (e.g., Dalcanton et al. 2009) have shown the wealth of information that can be obtained using resolved CMDs of stars within a galaxy. For comparison with such studies in the stochastic regime, SLUG produces binned 2 dimensional histograms that keep track of the user’s choice of color magnitude diagrams. Such diagrams allow us to directly characterize the effects of stochasticity in a coeval population. In Figure 8, we compare CMDs produced by SLUG for a $10^5 M_\odot$ instantaneous to

the theoretical isochrones from which they are produced. Aside from demonstrating we accurately reproduce the tracks, we are able to see the effects of stochasticity in leaving rapid phases of evolution unpopulated. Note that SLUG is capable of producing such diagrams for any given SFH.

5.2. Effects on Composite Populations

While individual clusters of stars can be treated as coeval, larger systems are intrinsically built of composite populations. One of the most basic composite populations one can consider is a galaxy forming stars at a constant star formation rate. As discussed in Section 2.2, the value of the SFR will have a significant impact on the effects of stochasticity.

To demonstrate the differences that stochasticity makes, we compare SLUG realizations to those of a well-sampled SB99 model. In Figure 9, we first examine the luminosities for SFRs of 1 , 10^{-1} , and $10^{-2} M_\odot \text{ yr}^{-1}$ with our fiducial values for the CMF and cluster mass fraction. For each SFR, we show the mean and median of the SLUG runs along with the 5 and 95 percentiles.

One can clearly see an increase in fractional scatter as one decreases the SFR, which can be attributed to the more bursty SFHs which are a result of the grouping of age in massive clusters. This scatter appears at higher SFRs than predicted by our naive discussion in Section 2.2 as a direct result of the clustering. In fact, nearly all of the scatter seen in Figure 9 is a result of the clustering rather than sampling of individual clusters. This is most clearly demonstrated by Figure 10 which shows similar simulations but with completely unclustered star forma-

tion. Without clustering the $10^{-2} M_\odot \text{ yr}^{-1}$ models have approximately an order of magnitude less scatter in the 5-95 percentile range of the log of the luminosity. We see that the unclustered stochastic effects behave as predicted in Section 2.2 where the fractional scatter is small for SFRs $\sim 10^{-2} M_\odot \text{ yr}^{-1}$ and quickly increases as the SFR decreases (also discussed in Fumagalli et al. 2011).

For a demonstration of the effects of clustering, we present the tracks of a subset of individual stochastic realizations of clustered star formation in Figure 11. One can see that the $Q(H^0)$ curves are less uniform than the R luminosity. This is a direct result of the sensitivity of $Q(H^0)$ to the youngest, most massive stars. One can also see that the scatter increases with decreasing SFR as expected. This is to be further discussed in da Silva et al. (in prep.) where we elaborate on the effects of stochastic star formation when one includes clusters.

6. SUMMARY

We introduce SLUG, a new code that correctly accounts for the effects of stochasticity (with caveats discussed in the text) by populating galaxies with stars and clusters of stars and then following their evolution using stellar evolutionary tracks. Cluster disruption is taken into account and a variety of outputs are created.

We present a series of tests comparing SLUG to observations and other theoretical predictions. SLUG is able to reproduce the photometric properties of clusters from the Larsen (1999) catalog as well as the Corbelli et al. (2009) birthline. It can also reproduce the results of SB99 in the well-sampled regime.

Finally we present SLUG outputs in the stochastic regime and demonstrate the flexibility of the code to address a variety of astrophysical problems with its variety of possible outputs.

SLUG is a publicly available code, and can be found at <http://sites.google.com/site/runslug/>.

R.L.d.S. is partially supported by an NSF CAREER grant (AST-0548180). The work of R.L.d.S. is supported under a National Science Foundation Graduate Research Fellowship. MRK acknowledges support from: an Alfred P. Sloan Fellowship; the National Science Foundation through grants AST-0807739 and CAREER-0955300; and NASA through Astrophysics Theory and Fundamental Physics grant NNX09AK31G and a *Spitzer Space Telescope* theoretical research program grant. We would like to thank J. X. Prochaska for help in reading and providing input on the early stages of this manuscript. We would like to thank F. Bigiel for encouraging us to create SLUG and useful conversations with J. Eldridge, C. Weidner, R. Bernstein, and J. Colucci.

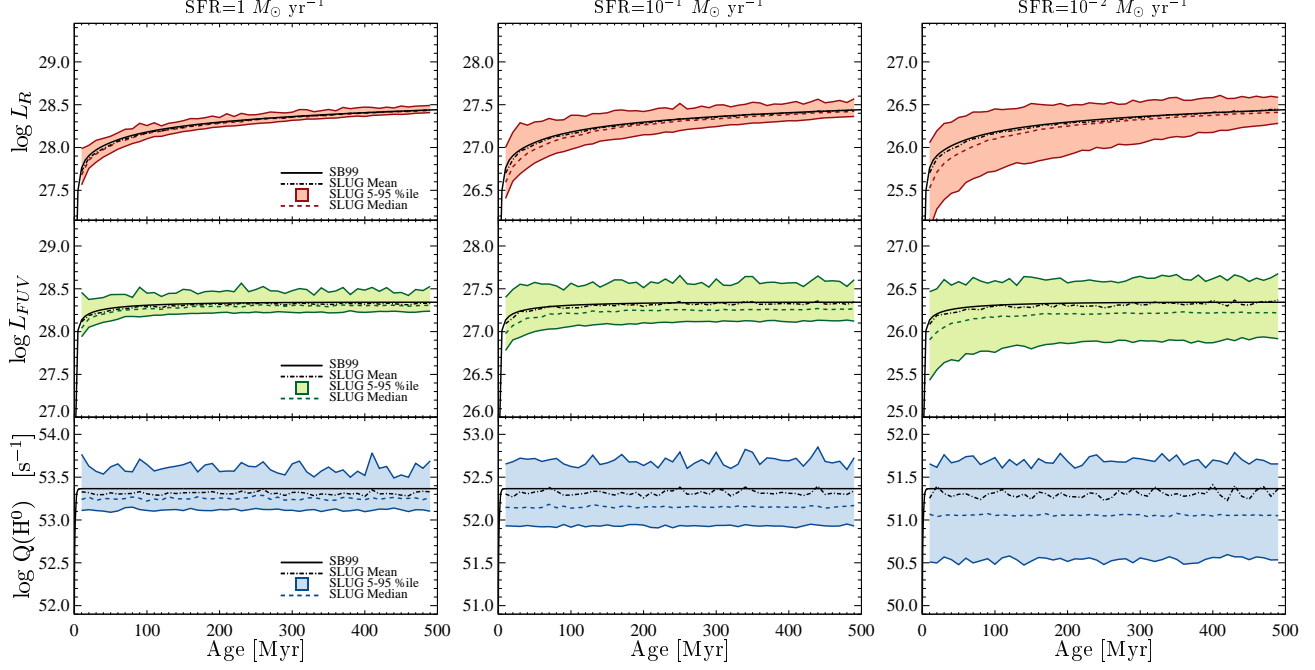


FIG. 9.— R -band, FUV, and ionizing photon luminosities vs. time for galaxies with constant SFRs of 1, 10^{-1} , and $10^{-2} M_{\odot} \text{ yr}^{-1}$ as indicated. R -band and FUV luminosities are in units of $\text{erg s}^{-1} \text{ Hz}^{-1}$. We compare a fully sampled realization from SB99 (solid black lines) with 100, 500, and 1000 realizations from SLUG for SFRs of 1, 10^{-1} , and $10^{-2} M_{\odot} \text{ yr}^{-1}$ respectively. The SLUG models are represented by their mean (black dash-dotted line), median (colored dashed line) and 5-95 percentile range (filled color region). Our SLUG models were set to only output every 10 million years. Note that the y-axis in each panel has been chosen to match the SFR, but always spans the same logarithmic interval.

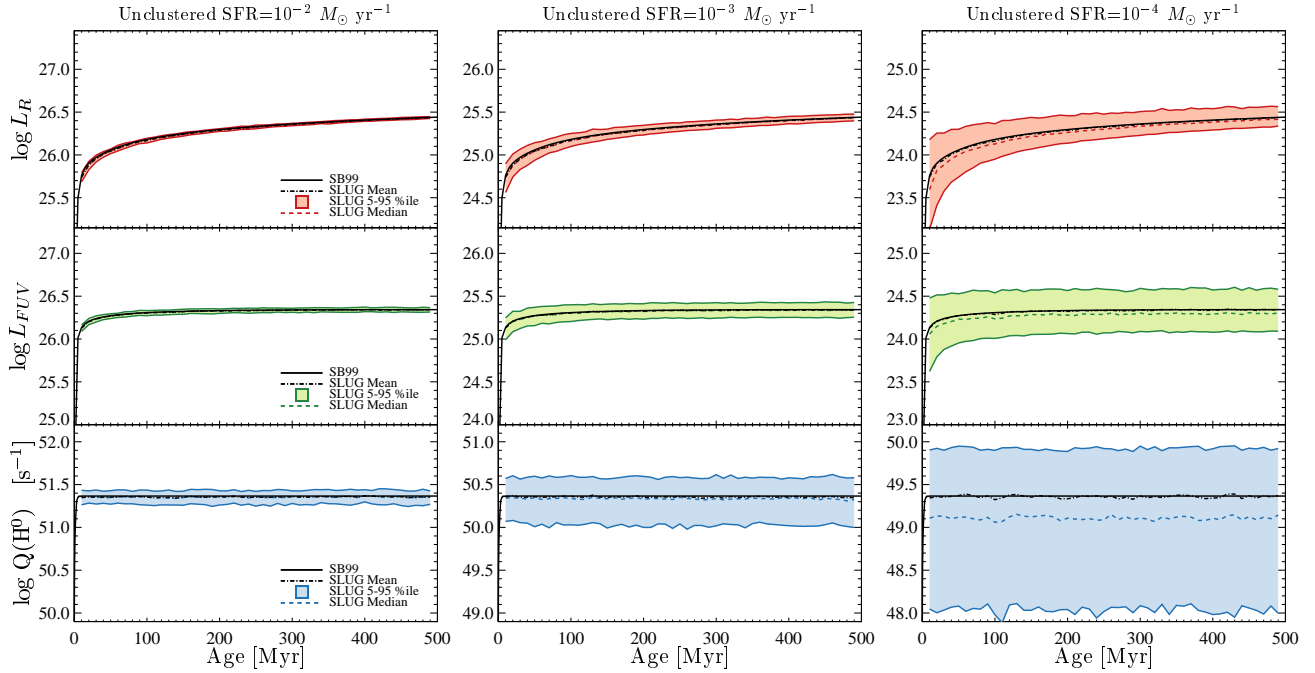


FIG. 10.— Same as Figure 9, but this time made with unclustered star formation, and using lower SFR. Note the third panel of Figure 9 is the same SFR as the first panel of this figure. These figures were constructed with 100, 500, and 1000 realizations at SFRs of 10^{-2} , 10^{-3} , and $10^{-4} M_{\odot} \text{ yr}^{-1}$ respectively.

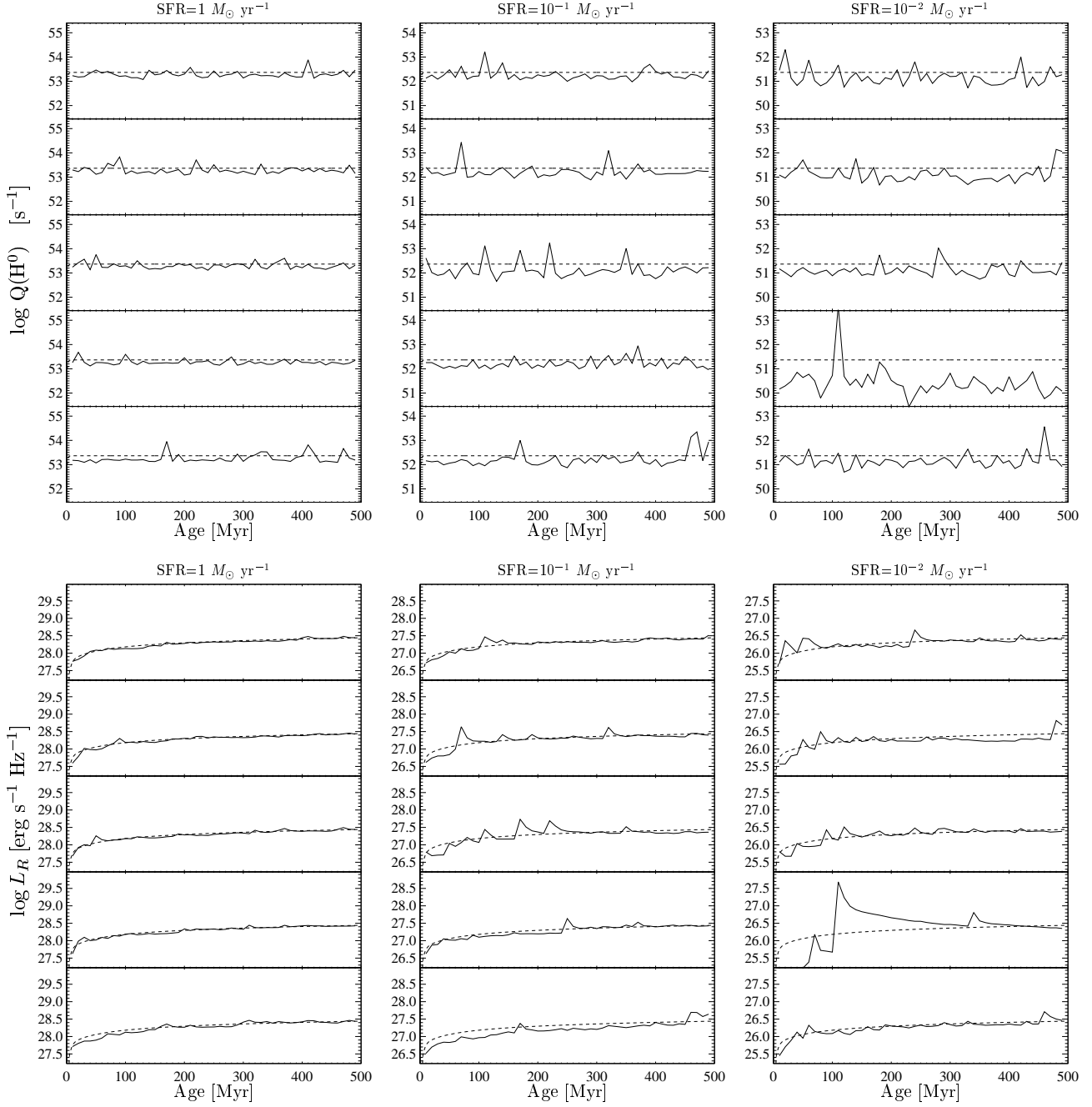


FIG. 11.— Solid lines show the evolution of $Q(\text{H}^0)$ and R band luminosity for individual simulations with clustered star formation with SFRs of 1, 10^{-1} , and $10^{-2} M_{\odot} \text{ yr}^{-1}$. Dashed lines show the SB99 prediction. Note that the y-axis in each panel has been chosen to match the SFR, but always spans the same logarithmic interval.

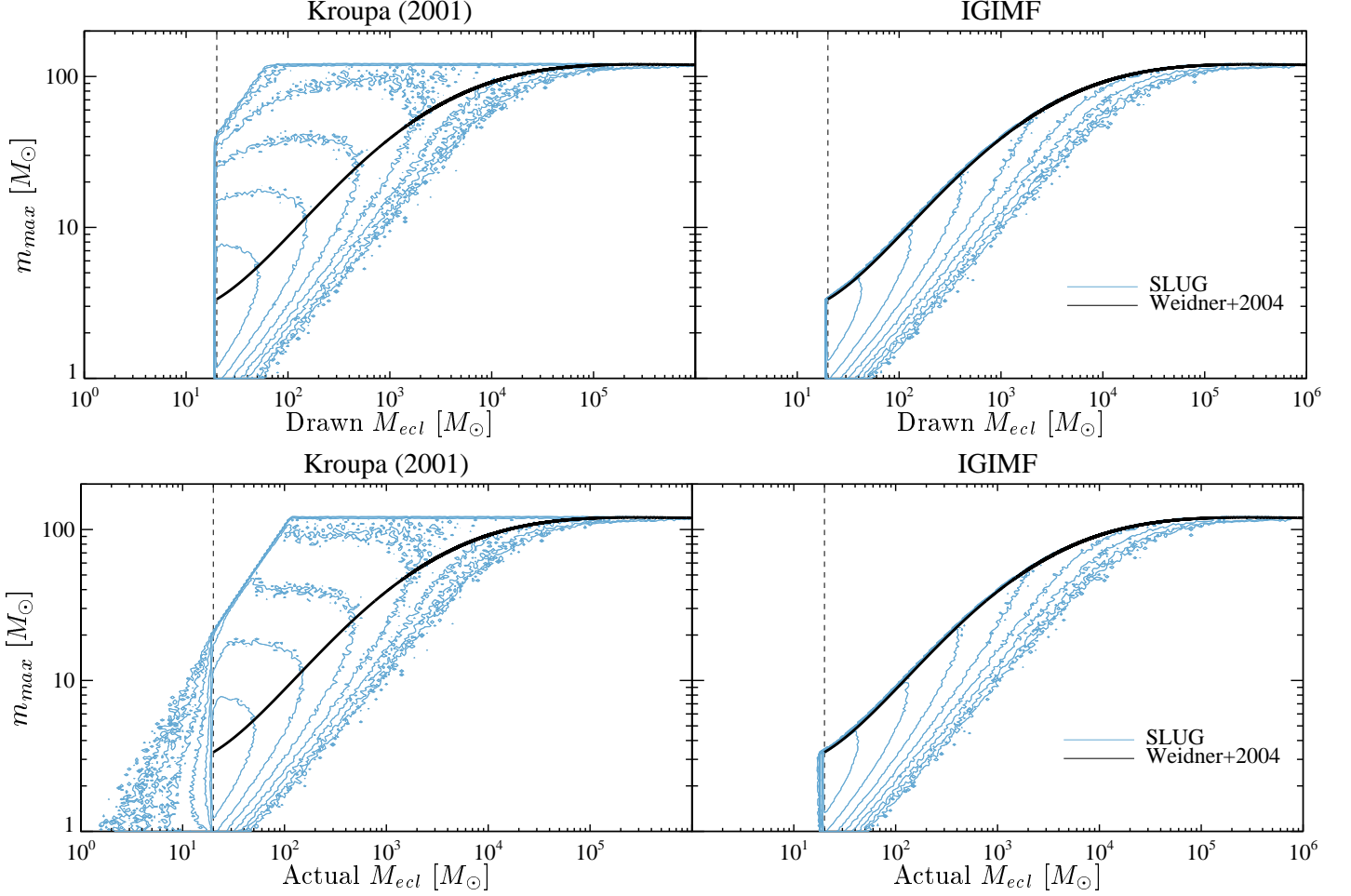


FIG. 12.— The mass of the largest star in a cluster vs. that cluster’s mass for clusters created by SLUG for a Kroupa (2001) IMF (*left*) and the IGIMF (*right*). The black lines denote the analytic prediction of the maximum possible stellar mass in a cluster in the IGIMF model, the black dashed line notes the lower limit of the cluster mass function, and blue contours denote the location of SLUG models. Top panels show the maximum stellar mass as a function of the cluster mass drawn from the CMF, while bottom panels show the same relation relative to the sum of the masses of all stars actually populating the clusters. These two differ slightly— see section 3.2.

APPENDIX

IMPLEMENTATION OF IGIMF

The IGIMF theory is a statement that the SFR controls the upper cutoff of the CMF and that each cluster’s mass changes the upper cutoff of the IMF in that cluster.

We implement the IGIMF following Weidner et al. (2010b). We use the work of Pflamm-Altenburg & Kroupa (2008), Weidner & Kroupa (2005), and Weidner et al. (2004) to define the maximum cluster mass as

$$M_{ecl,max} = 84793 \left(\frac{\langle \text{SFR} \rangle}{M_{\odot} \text{ yr}^{-1}} \right)^{3/4}, \quad (\text{A1})$$

where $\langle \text{SFR} \rangle$ is the time-average SFR. Thus the SFR affects the upper cut off of the CMF. We determine the average star formation rate over a time interval defined by the user (fiducially 10^7 yr).

After a cluster mass has been drawn, we must adjust the upper cutoff of the IMF that we use to draw stars for that cluster. The relation between maximum stellar mass and cluster mass ($m_{max} - M_{ecl}$) has been studied by Weidner & Kroupa (2004) and Weidner et al. (2010a). Following their treatment, we solve a system of equations numerically for m_{max} as a function of M_{ecl} .

The first equation is simply a statement that the total cluster mass (M_{ecl}) is the integral of the distribution of masses ($\frac{dN}{dm}$) integrated from the lowest to highest mass star in the cluster:

$$M_{ecl} = \int_{m_{min}}^{m_{max}} m \frac{dN}{dm} dm. \quad (\text{A2})$$

The next constraint is derived based on the statement that there is only one star in the cluster with mass equal to m_{max} . Their choice of implementation of this statement is as follows¹⁰:

$$1 = \int_{m_{max}}^{m_{max,*}} \frac{dN}{dm} dm \quad (A3)$$

where $m_{max,*}$ is the maximum stellar mass possible.

In the specific case of a Kroupa (2001) IMF, these equations reduce to the following (taken from Weidner & Kroupa 2004).

$$1 = k \left[\left(\frac{m_H}{m_0} \right)^{\alpha_1} \left(\frac{m_0}{m_1} \right)^{\alpha_2} m_1^{\alpha_3} \left(\frac{m_{max,*}^{1-\alpha_3}}{1-\alpha_3} - \frac{m_{max}^{1-\alpha_3}}{1-\alpha_3} \right) \right] \quad (A4)$$

$$\begin{aligned} \frac{M_{cl}}{k} = & \frac{m_H^{\alpha_0}}{2-\alpha_0} (m_H^{2-\alpha_0} - m_{low}^{2-\alpha_0}) + \frac{m_H^{\alpha_1}}{2-\alpha_1} (m_0^{2-\alpha_1} - m_H^{2-\alpha_1}) \\ & + \frac{\left(\frac{m_H}{m_0} \right)^{\alpha_2} m_0^{\alpha_2}}{2-\alpha_1} (m_1^{2-\alpha_2} - m_0^{2-\alpha_2}) + \frac{\left(\frac{m_H}{m_0} \right)^{\alpha_2} \left(\frac{m_0}{m_1} \right)^{\alpha_2} m_1^{\alpha_3}}{2-\alpha_3} (m_{max}^{2-\alpha_3} - m_0^{2-\alpha_3}) \end{aligned} \quad (A5)$$

where

$$\begin{aligned} \alpha_0 &= +0.30, \quad m_{low} = 0.01 \\ \alpha_1 &= +1.30, \quad m_H = 0.08 \\ \alpha_2 &= +2.30, \quad m_0 = 1.00 \\ \alpha_3 &= +2.35, \quad m_{max,*} = 120 \end{aligned} \quad (A6)$$

We fit a 6th order polynomial to the numerical solution to find:

$$\log_{10} m_{max} = \sum_{i=0}^6 a_i (\log_{10} M_{cl})^i \quad (A7)$$

where $a=[1.449, -2.522, 2.055, -0.616, 0.0897, -0.00643, 0.000182]$.

We then use this upper mass limit to modify the standard Kroupa (2001) IMF to fill in the stars for the cluster. Figure 12 demonstrates the result. One can see that we are accurately applying the cutoff to the IMF in the IGMF.

REFERENCES

- Appenzeller, I., et al. 1998, *The Messenger*, 94, 1
Bigiel, F., Leroy, A., Walter, F., Blitz, L., Brinks, E., de Blok, W. J. G., & Madore, B. 2010, *AJ*, 140, 1194
Boissier, S., et al. 2007a, *ApJS*, 173, 524
—, 2007b, *ApJS*, 173, 524
—, 2008, *ApJ*, 681, 244
Boselli, A., Boissier, S., Cortese, L., Buat, V., Hughes, T. M., & Gavazzi, G. 2009, *ApJ*, 706, 1527
Cerviño, M., & Luridiana, V. 2004, *A&A*, 413, 145
Cerviño, M., Luridiana, V., Pérez, E., Vílchez, J. M., & Valls-Gabaud, D. 2003, *A&A*, 407, 177
Cerviño, M., Perez, E., Sanchez, N., Roman-Zuniga, C., & Valls-Gabaud, D. 2010, *ArXiv e-prints*
Cerviño, M., & Valls-Gabaud, D. 2003, *MNRAS*, 338, 481
Chabrier, G. 2003, *PASP*, 115, 763
Chandar, R., Fall, S. M., & Whitmore, B. C. 2010, *ApJ*, 711, 1263
Charlot, S., & Bruzual, A. G. 1991, *ApJ*, 367, 126
Colucci, J. E., Bernstein, R. A., Cameron, S. A., & McWilliam, A. 2011, *ArXiv e-prints*
Conroy, C., & Gunn, J. E. 2010, *ApJ*, 712, 833
Conroy, C., Gunn, J. E., & White, M. 2009, *ApJ*, 699, 486
Conroy, C., White, M., & Gunn, J. E. 2010, *ApJ*, 708, 58
Corbelli, E., Verley, S., Elmegreen, B. G., & Giovanardi, C. 2009, *A&A*, 495, 479
Cordier, D., Pietrinferni, A., Cassisi, S., & Salaris, M. 2007, *AJ*, 133, 468
- Cerviño et al. (2010) have pointed out that this expression does not equate to the logical statement mentioned above—it underpredicts the maximum mass in 63% of cases. In fact, this formalism equates rather to the statement that the expectation value of stars in the interval $m_{max} - m_{max,*}$ is equal to 1. However this is the standard formalism of the IGMF, so it is the formalism we implement.
- Crowther, P. A., Schnurr, O., Hirschi, R., Yusof, N., Parker, R. J., Goodwin, S. P., & Kassim, H. A. 2010, *MNRAS*, 408, 731
Dalcanton, J. J., et al. 2009, *ApJS*, 183, 67
de Wit, W. J., Testi, L., Palla, F., Vanzani, L., & Zinnecker, H. 2004, *A&A*, 425, 937
de Wit, W. J., Testi, L., Palla, F., & Zinnecker, H. 2005, *A&A*, 437, 247
Eldridge, J. J., & Stanway, E. R. 2009, *MNRAS*, 400, 1019
Elmegreen, B. G. 2000, *ApJ*, 539, 342
Fagotto, F., Bressan, A., Bertelli, G., & Chiosi, C. 1994, *A&AS*, 105, 29
Fall, S. M., Chandar, R., & Whitmore, B. C. 2009a, *ApJ*, 704, 453
—, 2009b, *ApJ*, 704, 453
Fall, S. M., Krumholz, M. R., & Matzner, C. D. 2010, *ApJ*, 710, L142
Figer, D. F. 2005, *Nature*, 434, 192
Fioc, M., & Rocca-Volmerange, B. 1997, *A&A*, 326, 950
Fukugita, M., Ichikawa, T., Gunn, J. E., Doi, M., Shimasaku, K., & Schneider, D. P. 1996, *AJ*, 111, 1748
Fumagalli, M., da Silva, R., Krumholz, M., & Bigiel, F. 2010, *ArXiv e-prints*
Fumagalli, M., da Silva, R. L., & Krumholz, M. R. 2011, *ArXiv e-prints*
Fumagalli, M., & Gavazzi, G. 2008, *A&A*, 490, 571
Gogarten, S. M., et al. 2009, *ApJ*, 691, 115
Haas, M. R., & Anders, P. 2010, *A&A*, 512, A79+
Hillier, D. J., & Miller, D. L. 1998, *ApJ*, 496, 407
Hirashita, H., Buat, V., & Inoue, A. K. 2003, *A&A*, 410, 83
Hosokawa, T., Offner, S. S. R., & Krumholz, M. R. 2011, *ArXiv e-prints*
Hoversten, E. A., & Glazebrook, K. 2008, *ApJ*, 675, 163
Jeffries, R. D. 2007, *MNRAS*, 381, 1169
Kotulla, R., Fritze, U., Weilbacher, P., & Anders, P. 2009, *MNRAS*, 396, 462

- Kroupa, P. 2001, *MNRAS*, 322, 231
- Kroupa, P., & Weidner, C. 2003, *ApJ*, 598, 1076
- Lada, C. J., & Lada, E. A. 2003, *ARA&A*, 41, 57
- Lamb, J. B., Oey, M. S., Werk, J. K., & Ingleby, L. D. 2010, *ApJ*, 725, 1886
- Larsen, S. S. 1999, *A&AS*, 139, 393
- Lee, J. C., Kennicutt, R. C., Funes, José G., S. J., Sakai, S., & Akiyama, S. 2007, *ApJ*, 671, L113
- Lee, J. C., et al. 2009, *ApJ*, 706, 599
- Leitherer, C., & Heckman, T. M. 1995, *ApJS*, 96, 9
- Leitherer, C., Robert, C., & Drissen, L. 1992, *ApJ*, 401, 596
- Leitherer, C., et al. 1999, *ApJS*, 123, 3
- Lejeune, T., Cuisinier, F., & Buser, R. 1997, *A&AS*, 125, 229
- . 1998, *A&AS*, 130, 65
- McKee, C. F., & Williams, J. P. 1997, *ApJ*, 476, 144
- Meurer, G. R., et al. 2009, *ApJ*, 695, 765
- Meynet, G., Maeder, A., Schaller, G., Schaerer, D., & Charbonnel, C. 1994, *A&AS*, 103, 97
- Mollá, M., García-Vargas, M. L., & Bressan, A. 2009, *MNRAS*, 398, 451
- Morrissey, P., et al. 2005, *ApJ*, 619, L7
- Oey, M. S., King, N. L., & Parker, J. W. 2004, *AJ*, 127, 1632
- Osterbrock, D. E., & Ferland, G. J. 2006, *Astrophysics of gaseous nebulae and active galactic nuclei*, ed. Osterbrock, D. E. & Ferland, G. J.
- Palla, F., & Stahler, S. W. 1999, *ApJ*, 525, 772
- Pauldrach, A. W. A., Hoffmann, T. L., & Lennon, M. 2001, *A&A*, 375, 161
- Pflamm-Altenburg, J., & Kroupa, P. 2008, *Nature*, 455, 641
- Pietrinferni, A., Cassisi, S., Salaris, M., Cordier, D., & Castelli, F. 2007, in *IAU Symposium*, Vol. 241, *IAU Symposium*, ed. A. Vazdekis & R. F. Peletier, 39–40
- Reines, A. E., Nidever, D. L., Whelan, D. G., & Johnson, K. E. 2010, *ApJ*, 708, 26
- Salpeter, E. E. 1955, *ApJ*, 121, 161
- Schlegel, D. J., Finkbeiner, D. P., & Davis, M. 1998, *ApJ*, 500, 525
- Schmutz, W. 1998, in *Astronomical Society of the Pacific Conference Series*, Vol. 131, *Properties of Hot Luminous Stars*, ed. I. Howarth, 119–+
- Skrutskie, M. F., et al. 2006, *AJ*, 131, 1163
- Thilker, D. A., et al. 2007, *ApJS*, 173, 538
- Vázquez, G. A., & Leitherer, C. 2005, *ApJ*, 621, 695
- Weidner, C., & Kroupa, P. 2004, *MNRAS*, 348, 187
- . 2005, *ApJ*, 625, 754
- Weidner, C., Kroupa, P., & Bonnell, I. A. D. 2010a, *MNRAS*, 401, 275
- Weidner, C., Kroupa, P., & Larsen, S. S. 2004, *MNRAS*, 350, 1503
- Weidner, C., Pflamm-Altenburg, J., & Kroupa, P. 2010b, *ArXiv e-prints*
- Weisz, D. R., Skillman, E. D., Cannon, J. M., Dolphin, A. E., Kennicutt, Jr., R. C., Lee, J., & Walter, F. 2008, *ApJ*, 689, 160
- Werk, J. K., Putman, M. E., Meurer, G. R., Oey, M. S., Ryan-Weber, E. V., Kennicutt, Jr., R. C., & Freeman, K. C. 2008, *ApJ*, 678, 888
- Zhang, Q., & Fall, S. M. 1999, *ApJ*, 527, L81